E&P / Tommi Rämä

16 January 2025 NUCL-5017

Distribution

Reviewed by, Date
Timo Toppila 16.1.2025

Approved by, Date
Olli Viljakainen 16.1.2025

Electronically reviewed and approved original is in Fortum ProjectWise-program.

Replace

SAFER2024, CERESA SUBPROJECT
SIMULATION OF A SELECTED PNL EXPERIMENT

TABLE OF CONTENTS

E&P / Tommi Rämä 16 January 2025 NUCL-5017

1 INTRODUCTION

The containment of a Pressurized Water Reactor (PWR) serves as the final barrier against the release of radioactive materials in the event of an accident or malfunction within the reactor core. Understanding and analyzing this containment system is essential to safeguarding the well-being of not only the workers at the nuclear facility but also the public at large. Containment analysis plays a pivotal role in assessing and enhancing the resilience of these structures, thereby minimizing the risk of catastrophic incidents and mitigating the consequences of severe accidents.

The containment analyses at Fortum have been carried out with MELCOR and APROS system codes. Now that the detailed three-dimensional CFD (Computational Fluid Dynamics) codes and the computer power developed rapidly over the last years, the application of CFD for reactor scale containment analyses has become possible.

2 CONTAINMENT MODEL

The main goal of the CeReSa-subproject is to model hydrogen behaviour in NPP containments with CFD. In order to find out the most important phenomena that needs to be taken into account, Phenomena Identification and Ranking Table (PIRT) was made based on a hypothetical LOCA accident on Loviisa VVER-440 NPP to guide the model development. Input for ranking was asked from project personnel, SAFER TAG 2.1 and other stakeholders. Readiness of the OpenFOAM models is based on the view of the project personnel, as well as the timetable for the model development. Table is reviewed version of from previous year (Rämä 2024). The ranking, readiness and the timetable are shown below in Table 1.

Table 1. Phenomena identification ranking table and their readiness of the OpenFOAM models. Year on the right indicates the year when the model is scheduled to be implemented (if at all).

Table 1: Phenomena Identification and Ranking Table for a hypothetical LOCA accident in Loviisa VVER-440 NPP.

	Ranking by weighted average	Readiness Ready Needs some work Needs to be implemented Implemented in another project	Timetable
Condensation at ice surfaces.	3.00		2023
Ice melting.	3.00		2024
Stratification.	3.00		-
Thermal mixing.	3.00		-
Recombiners.	3.00		2025 (or not at all)
Effect of non-condensable gases on condensation.	3.00		2023
Effect of non-condensable gases on stratification.	2.83		-
Igniters.	2.83		2025 (or not at all)
Hydrogen combustion.	2.83		2025
Condensation on walls.	2.67		2023
Turbulence modelling.	2.67		-
Heat transfer between fluids and structures.	2.50		2023
Pressure losses in ice condenser.	2.33		2024
Water pools.	2.33		2024
Bulk condensation.	2.20		2024
Mist formation/evaporation.	2.17		2025
Behaviour of gas/liquid surfaces.	2.17		2024
Aerosol transport and deposition.	2.00		Not at all
Condensation on the water pools.	2.00		2024
Water films at surfaces.	1.83		2024
Thermal radiation.	1.83		-
Water droplets.	1.80		2024
Mist rainout.	1.67	No model needed.	-
Dissolution of the hydrogen.	1.50		Not at all
Mist deposition.	1.50		Not at all

In 2023 the OpenFOAM development work in CeReSa project was focused on the surface condensation (Syrjänen & Hovi 2023), and in 2024 water film and ice condenser models (Niemi et al. 2024). For the modelling of the ice condenser correctly the pressure loss, ice melting and bulk condensation are important, see Table 1.

3 CFD MODEL DESCRIPTION

In this report simulations are made with Ansys Fluent CFD model. The same surface condensation models as in Rämä (2024) are used. In addition, earlier developed ice condenser models (Siccama 2015) used for example in Rämä et al. (2019) are also included, as the focus is on the behaviour of the ice condenser models.

The best way to assess and improve the ice condenser modelling is to use full height ice condenser experiments available to validate the models. In this report simulations are compared against an experiment made by Pacific Northwest National Laboratory and sponsored by NRC (Ligotke et al. 1991). In the future the results can also be compared against the OpenFOAM simulations by Niemi et al. (2024)

3.1 Geometry

Used geometry is the same as in reference Niemi et al. (2024). The geometry information of the model were from Ligotke et al. (1991). With some exact values missing, below mentioned issues were tackled using engineering judgement and general figures available in the document.

1. Length from the pipe bend to diffuser.
2. Length between diffuser and the ice condenser downcomer.
3. Height of the ice condenser downcomer.
4. Number, locations and dimensions of the guiding vanes at the bottom and top of the ice condenser

General view of the model geometry is presented in Figure 1.

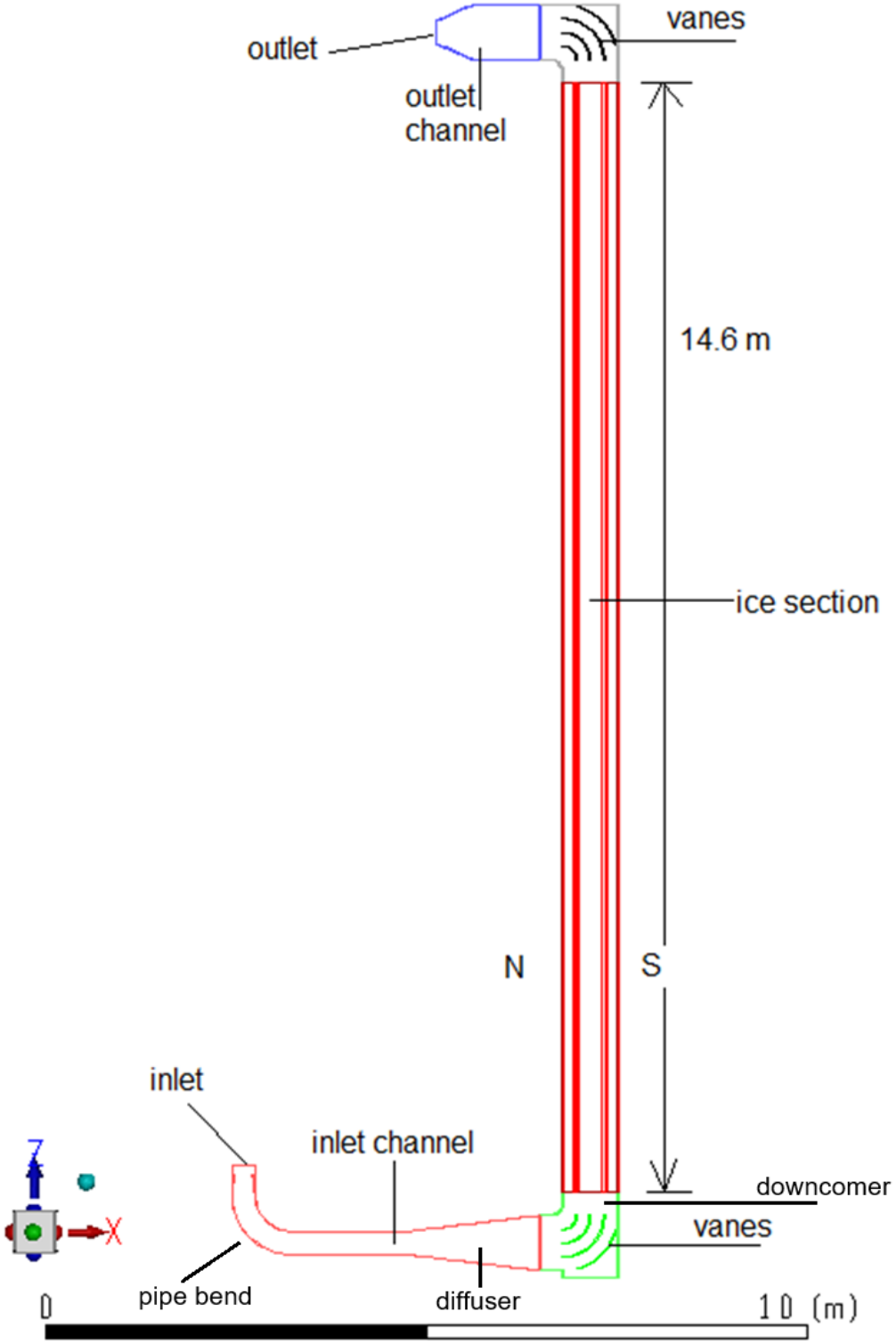

Figure 1. Geometry of the modelled domain. View from the west. N refers to northern wall and S to southern wall.

3.2 Computational grid

The computational mesh was generated using commercial Ansys Fluent Meshing tool. Grid consists of tetrahedral, heksahedral and wedge cells. Total amount of the cells is 52000, of which 400 is in the ice condenser section.

Because the ice condenser model used in this study is based on porous medium approach, where it is assumed that there is ice and air present in every cell, the mesh in the ice condenser section should be fairly coarse in the horizontal direction. The ice condenser was divided into four cells in horizontal direction, presenting the four subchannels in the test facility (see Figure 2 and Figure 9). In Figure 5 and Figure 6 the computational mesh on the vertical plane y=0 m and in ice condenser section are shown.

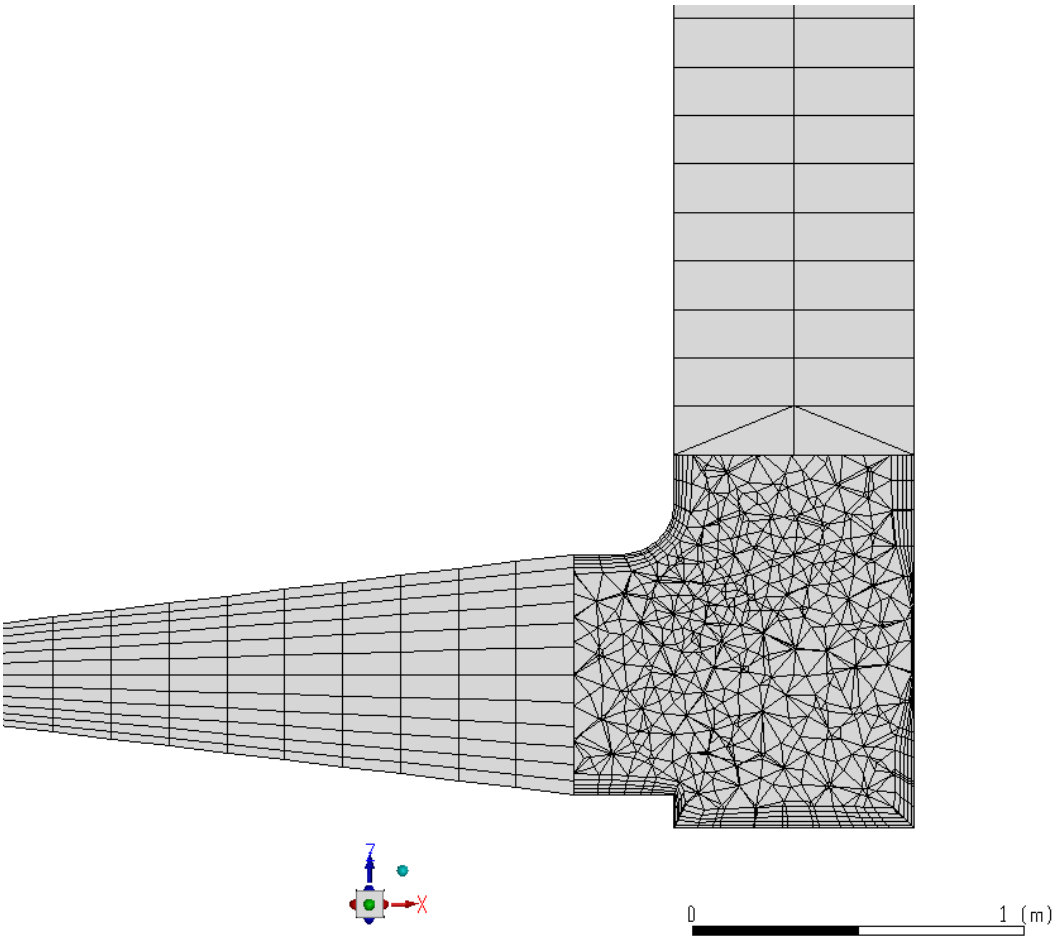

Figure 2. Computational grid, *mesh02*, at the middle plane of the modelled domain.

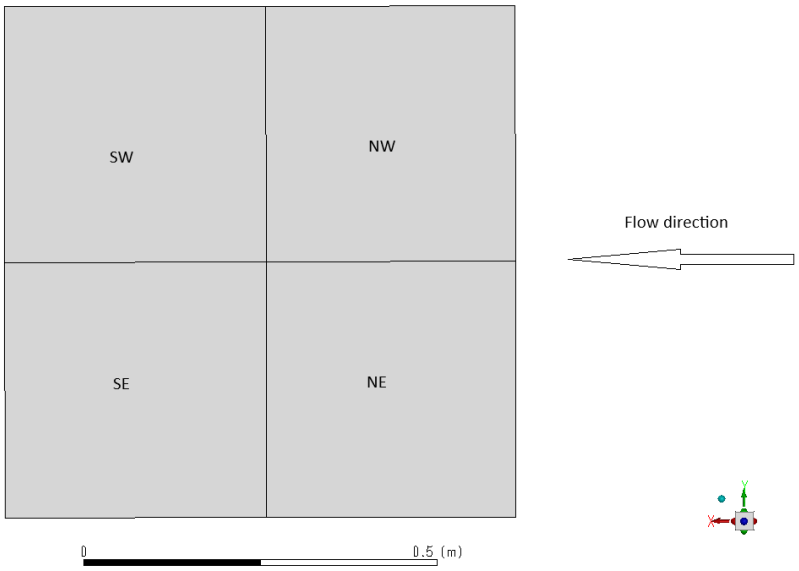

Figure 3. Computational grid, *mesh02*, at a horizontal plane intersecting the ice condenser.

Table 2. Mesh parameters.

Mesh cells	Cells in IC	Cell size in IC (m^3)	Min cell size outside IC (m^3)	Max cell size outside IC (m^3)
51 763	400	0.02	$2.7 \cdot 10^{-7}$	$1.1 \cdot 10^{-3}$

3.3 Physical and numerical models

Ansys Fluent solver version 2024R2 was used for the simulations. It solves basic fluid flow, temperature and turbulence fields and species transport. (Ansys 2024) In addition solving the following phenomena was addressed via user-defined-functions (UDFs) (Siccama 2015):

- wall deposition and evaporation
- bulk condensation and evaporation
- mist formation and rainout
- ice melting
- deposition on ice

In this report the water film behaviour is neglected. Single-phase modelling, with condensation modelled with volumetric and wall reactions, was used. Steam, mist and air were modelled as different species.

Numerical solver models were selected according to references (Siccama 2015, Visser 2015a and Visser 2015b). For pressure-velocity coupling *PISO* scheme, with

Skewness Correction 1 and *Neighbor Correction* 1, is applied. For pressure *Body Force Weighted* scheme is applied. For all other variables *Second Order Upwind* method is used. Turbulence is modelled with *standard k-ε* model with enhanced wall treatment. Analyses are made with transient solver with a time-step gradually increasing from 0.01 s to 1 s.

3.4 Material properties

Temperature dependent material properties based on Visser (2015b) were used for vapour, mist and deposited water. Temperature dependent material properties from Incropera&DeWitt (1996) were used for air.

Table 3. Properties of water-vapor.

Temperature (K)	Specific heat (J/(kg·K))	Thermal conductivity (W/(m·K))	Viscosity (kg/(m·s))
290	1902.3	0.018031	$0.9641 \cdot 10^{-5}$
380	2053.2	0.025561	$1.2525 \cdot 10^{-5}$
500	1981.6	0.035865	$1.7269 \cdot 10^{-5}$
600	2026.9	0.046368	$2.1407 \cdot 10^{-5}$

Table 4. Properties of air.

Temperature (K)	Specific heat (J/(kg·K))	Thermal conductivity (W/(m·K))	Viscosity (kg/(m·s))
290	1007	0.0255	$1.81 \cdot 10^{-5}$
450	1022	0.0363	$2.51 \cdot 10^{-5}$
600	1052	0.0457	$3.07 \cdot 10^{-5}$

4 SIMULATION CASE

Used boundary and initial conditions were chosen according to experiment in question from reference (Ligotke et al. 1991). Volume flows were converted to mass flow according to inlet temperature and pressure level of 101 kPa (see also section 3.5). For the missing parameters engineering judgement was used.

Boundary conditions were as follows: Volume flow rates of 0.12 m3/s for air and 0.1 m3/s for steam were converted to mass flows of 0.105 kg/s for air and 0.05542 kg/s for steam at the inlet. Temperature for both was 126°C. Walls were modelled as adiabatic, as no information of the outside temperature, wall material or insulation was reported.

The maximum gauge pressure at the test facility was reported to be 13.1 kPa. For this simulation pressure level of 101 kPa was used. Initial temperature of -6°C was assumed for the 2480 kg/s of ice with the density of 597.5 kg/m^3. Ice condenser section was initialised to -6.7°C and other volumes to 20°C, both in 50% humidity.

5 RESULTS

The comparison sections used were selected according to the measurement information available in Ligotke et al. (1991). The locations of the comparison points are presented in Figure 4.

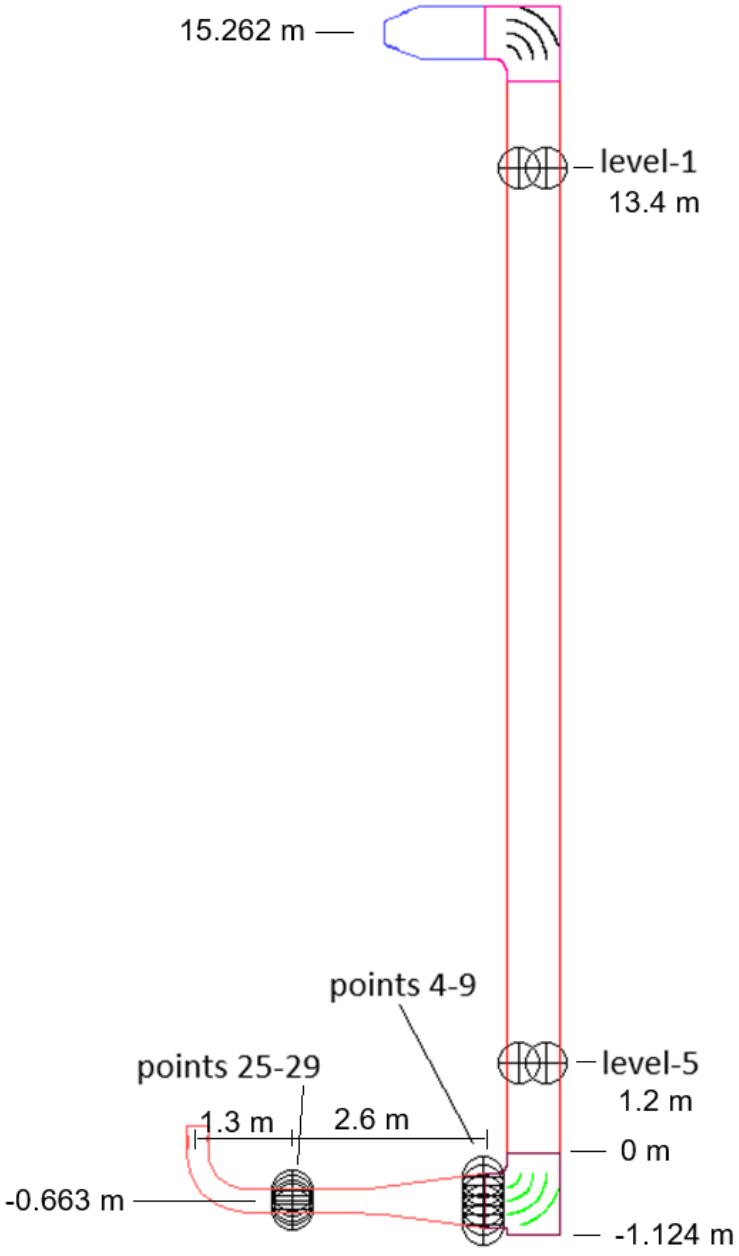

Figure 4. Location of the comparison points.

Temperature comparisons of the simulated case and measured values of the experiment 8 at the horizontal duct of the test facility is shown in Figure 5.

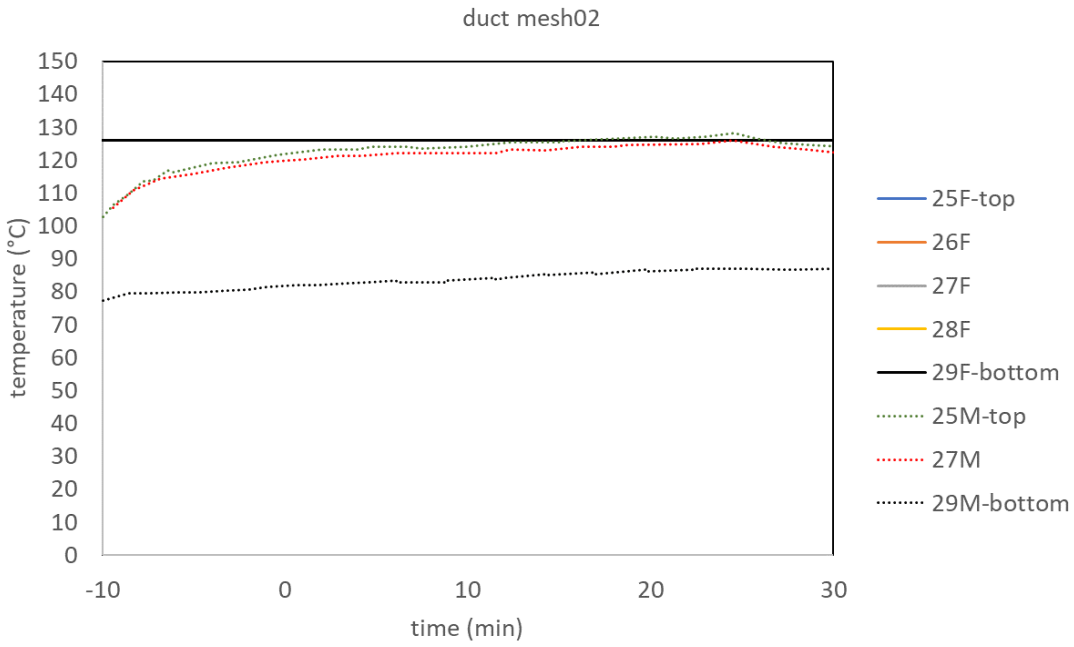

Figure 5. Temperature profiles at the inlet channel. Experiments with dashed lines (M) and simulations with solid lines (F). The location of the measurement points is shown in Figure 4.

Due to the adiabatic wall boundary condition the temperatures stay at the inlet temperature throughout the modelling period. In the experiment the temperature at the square duct before the diffuser is close to the inlet temperature excluding the lowest measurement point, where the temperature is significantly lower (80°C). The lower temperature at the bottom point might implicate that there is significant backward flow from the ice condenser all the way through the whole length of the diffuser. However, in the simulation the diffuser temperatures are lower than the measured ones, but the backward flow does not reach the horizontal duct region (see Figure 6). Thus the probable explanation for the lower temperature at the lowest measurement point is that there are significant heat losses through the bottom wall or that there is something wrong with the measurement.

E&P / Tommi Rämä 16 January 2025 NUCL-5017

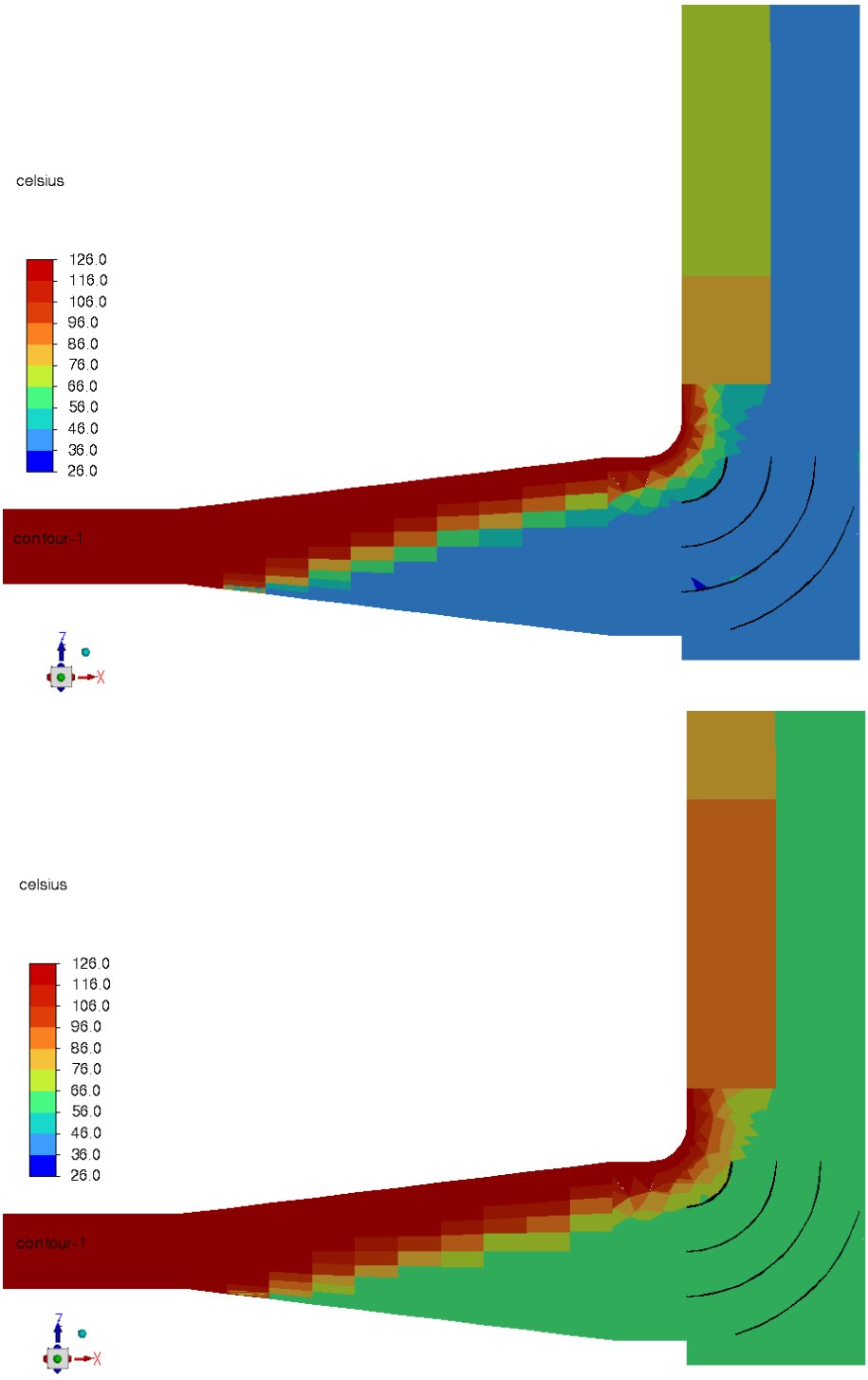

Figure 6. Temperature (°C) at the middle section of the horizontal flow channel and ice section at time 0 minutes (above) and at time 30 minutes (below).

Temperature comparisons of the simulated case and measured values of the experiment 8 at the diffuser outlet of the test facility is shown in Figure 7.

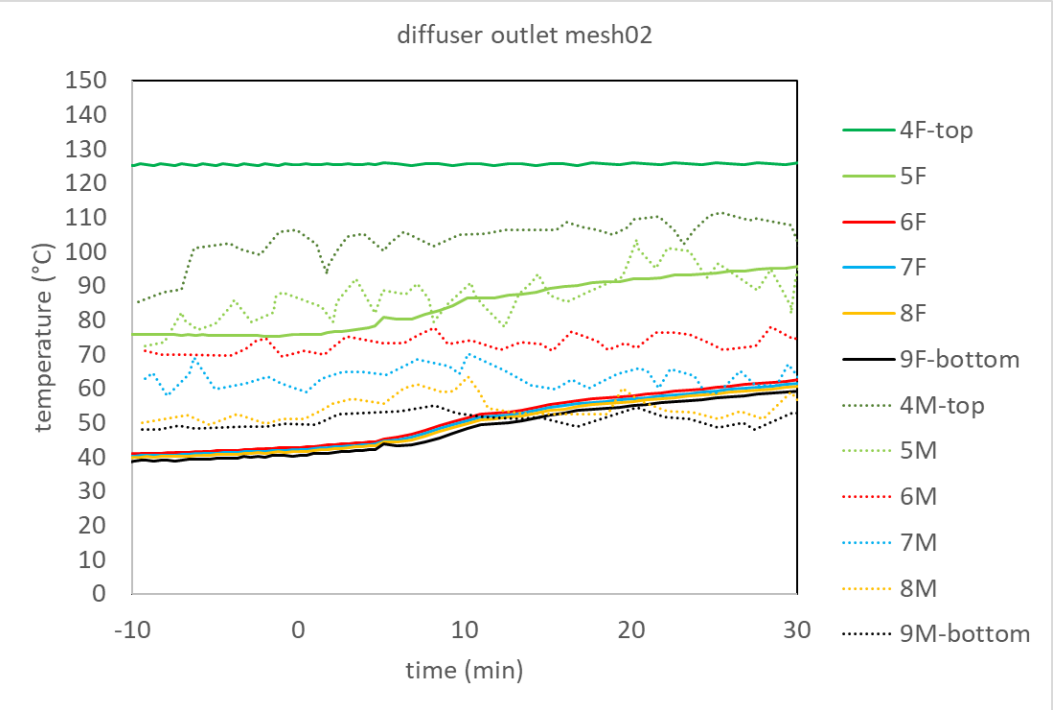

Figure 7. Temperature profiles at the diffuser outlet. Experiments with dashed lines (M) and simulations with solid lines (F). The location of the measurement points is shown in Figure 4.

There is clear temperature stratification at the diffuser outlet, both in the experiment and in the simulation results. This is due to the backflow from the ice condenser to the diffuser. In the experiment the temperature from up to down changes fairly evenly, whereas in the simulation the lowest four points have clearly lower temperature than other measurement points. In the experimental report it is mentioned, that circulation takes place only at the bottom part of the ice condenser, whereas in the simulation a large whirl of the whole ice section is generated, see Figure 8.

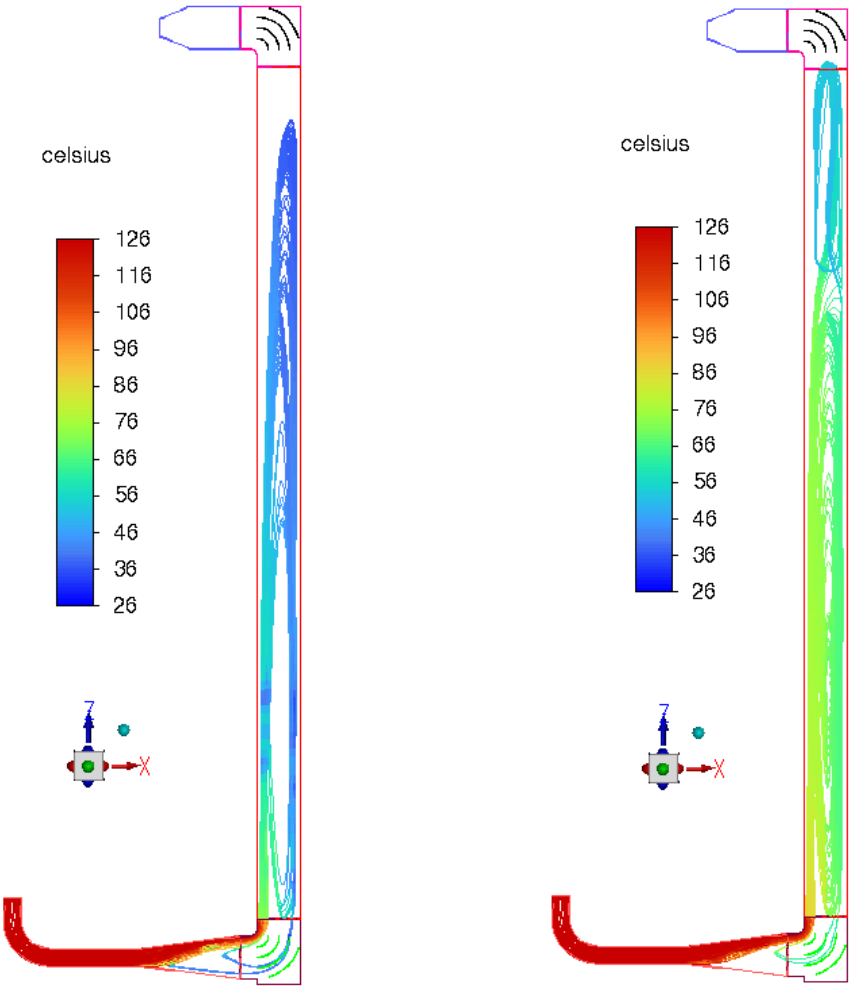

Figure 8. Pathlines at the middle of the horizontal flow channel and ice section at times 0 minutes (left) and 30 minutes (right).

It is assumed that due to the larger whirl the colder mixture flows longer way back to the diffuser, see Figure 6. There is also upwards trend in the simulation results, when in the experiment the temperature trends have stabilized.

Temperature comparisons of the simulated case and measured values of the experiment 8 at the ice condenser level 5 is shown in Figure 9.

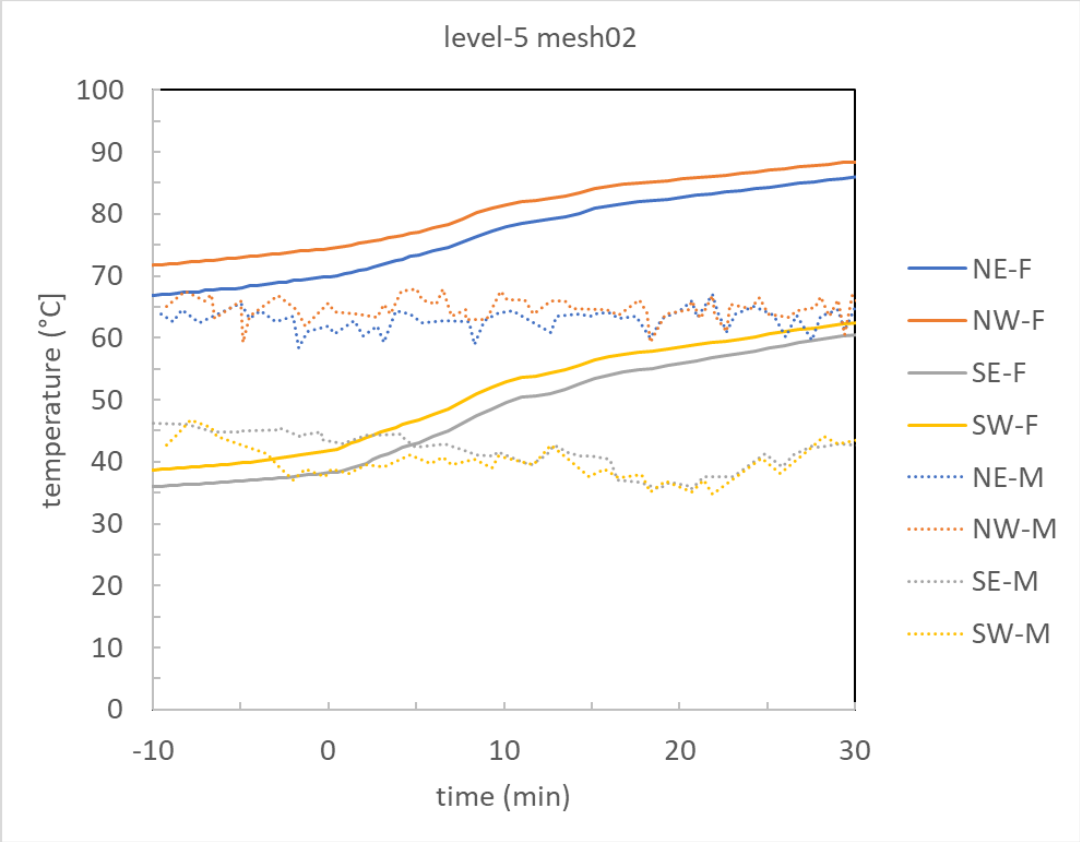

Figure 9. Temperature profiles at level 5 on elevation 1.2 meters above the ice condenser inlet. Experiments with dashed lines and simulations with solid lines. The location of the measurement points is shown in Figure 4.

In the measurements the temperatures at the NE and NW quadrants at level 5 are higher than in the SE and SW quadrants (see Figure 3), referring that the hot air-steam mixture flows upwards along the northern wall and pushes colder air downwards along the southern wall of the ice condenser section (see Figure 1). Similar behavior is repeated in the simulation. However, in the simulation there is a rising trend in the temperature, whereas in the experiment temperatures stay fairly constant. One reason for this might be that in the experiments the ice slides downwards inside the ice baskets cooling the bottom part. Another reason might be that the raindrop from the condensing steam and melting ice cools down the gas inflow. Both of these phenomena are missing from the simulation model.

Temperature comparisons of the simulated case and measured values of the experiment 8 at the ice condenser level 1 is shown in Figure 10.

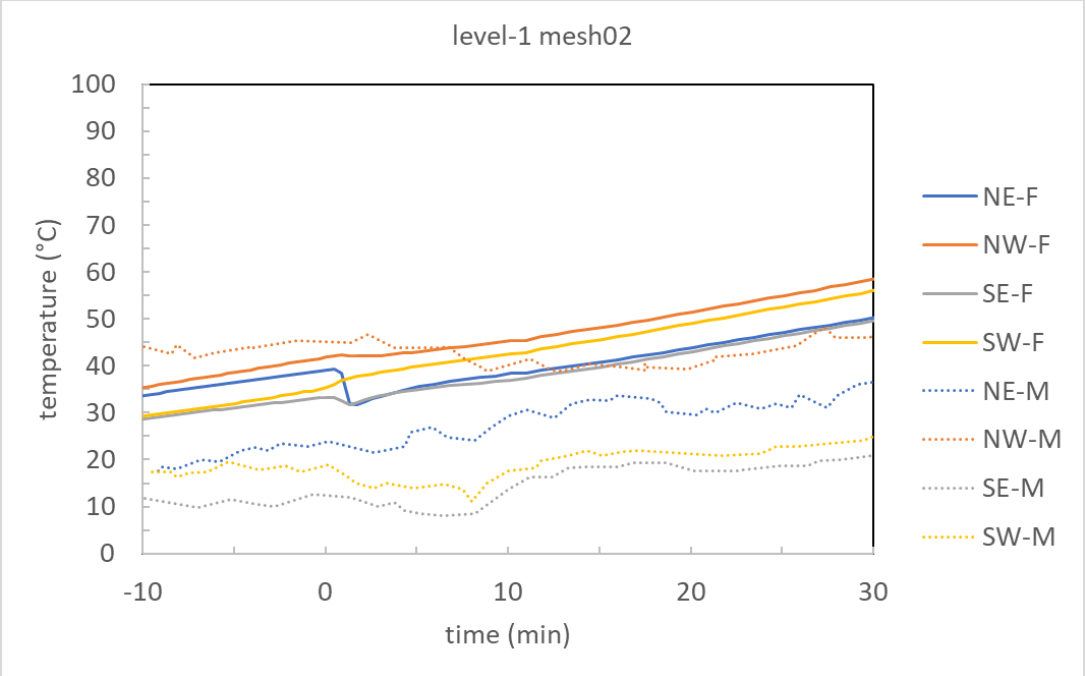

Figure 10. Temperature profiles at level 1 on elevation 13.4 meters above the ice condenser inlet. Experiments with dashed lines and simulations with solid lines. The location of the measurement points is shown in Figure 4.

At level 1 the temperatures at quadrants NE and NW are also at higher level than in the southern quadrants. In the experiments the temperature of the warmest quadrant, NW, stays at fairly constant level whereas the temperatures of the other quadrants slightly increase.

In the simulation the temperatures at quadrants NE and NW are also at higher level than in the southern quadrants. At time 0 minutes there is a clear change in the simulation flow field, because the temperatures at NE and SE drop, but the temperature at the SW increases, suggesting that there is a change in the flow field. The difference between warmest and coolest quadrants stays fairly constant throughout the simulated time. In the simulations the temperatures rise throughout the simulation period. The temperatures at the simulation are higher than the measured ones, which is in-line with the temperatures observed at level-5 (see Figure 10).

Steam mole fraction (SMF) at inlet and outlet measurement points, 6A and 0, respectively, were measured in the experiment 8. For comparison, the steam mole fractions from the model inlet and outlet were reported for the simulation. Results are presented in Figure 11.

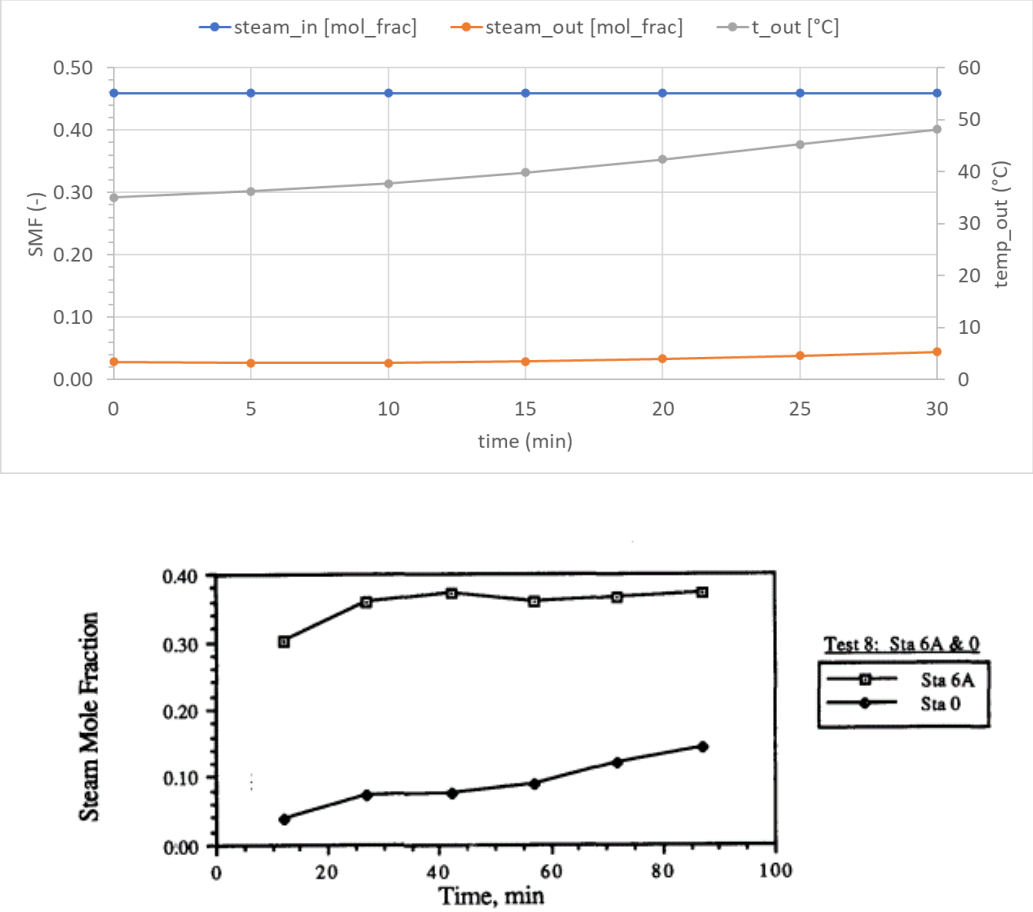

Figure 11. Steam mole fractions on the experiment 8 (Ligotke et al. 1991) on the inlet and outlet measurement stations, Sta 6A and Sta 0, respectively. Simulated values for the comparison are taken from the model inlet (blue) and outlet (orange). Simulated values above and measured below.

The steam mole fraction at the inlet measurement station of the experiment is lower than that calculated from the reported inlet flow rates. Thus it is likely, that either part of the steam is condensated already before the inlet measurement station, the reported inlet values are incorrect or that there is error in the measurements.

6 CONCLUSIONS

Several uncertainties regarding the geometry and boundary conditions make the quantitative comparison between the simulations and experiments difficult. However, it is possible to make qualitative comparison of how the used models work in general.

Compared to the measurement, the gas temperatures are too high in the ice condenser section, both at the bottom level and at the top level, but too low on the diffuser outlet. This suggests that the gas flows too easily upwards inside the ice condenser. One reason might be that the neglecting the effect of the droplets and ice falling inside the ice baskets leads to too low condensation in the model.

7 REFERENCES

ANSYS Fluent, 2024. ANSYS Fluent User's Guide. Release 2024R2. ANSYS, Inc. www.ANSYS.com.

Incropera, F. P., DeWitt, D. P. 1996. Fundamentals of Heat and Mass Transfer, 4th edition. Yhdysvallat: John Wiley & Sons,. 866 s. ISBN 0-471-30460-3.

Ligotke, M.W., Eschbach, E.J., Winegardner, W.K. 1991. Ice-Condenser Aerosol Tests. Report NUREG/CR-5768. U.S. NRC.

Niemi, T., Syrjänen, J., Hovi, V. 2024. Validation of a CFD model for PWR containment analysis. VTT Research report VTT-R-00338-24. VTT Technical Research Centre of Finland Ltd.

Rämä, T., Toppila, T., Visser, D.C., Siccama, N.B. 2019. Validation of ice condenser model for CFD analysis of VVER-440 type containment. Nuclear Engineering and Design volume 352. Elsevier B.V. https://doi.org/10.1016/j.nucengdes.2019.110163.

Rämä, T. 2024. SAFER2023, CeReSa subproject, Simulations of the selected CONAN experiments with Ansys Fluent. Fortum Report NUCL-4846. Fortum Power and Heat Oy.

Siccama, N.B. 2014. Fortum Ice Condenser Model in Fluent. NUCLEARRD-4-2659. Fortum Power and Heat Oy.

Syrjänen, J., Hovi, V. 2023. Validation of the surface condensation model for PWR containment analysis. VTT Research report VTT-R-00884-23. VTT Technical Research Centre of Finland Ltd.

Visser, D. 2015a. Validation of CFD Model against Victoria Experiment-27. CFD Model Validation. NUCLEARRD-4-2511. Fortum Power and Heat Oy.

Visser, D. 2015b. Validation of CFD Model against Victoria Experiment-44. CFD Model Validation. NUCLEARRD-4-2536. Fortum Power and Heat Oy.